Journal of
Mechanics of
Materials and Structures

EXACT CLOSED-FORM SOLUTION OF THE DYNAMIC COUPLED THERMOELASTIC RESPONSE OF A FUNCTIONALLY GRADED TIMOSHENKO BEAM

Mostafa Abbasi, Mehdy Sabbaghian and M. Reza Eslami

Volume 5, № 1 January 2010

mathematical sciences publishers

JOURNAL OF MECHANICS OF MATERIALS AND STRUCTURES
Vol. 5, No. 1, 2010

EXACT CLOSED-FORM SOLUTION OF THE DYNAMIC COUPLED THERMOELASTIC RESPONSE OF A FUNCTIONALLY GRADED TIMOSHENKO BEAM

MOSTAFA ABBASI, MEHDY SABBAGHIAN AND M. REZA ESLAMI

We present the analytical solution for a beam made of a functionally graded material based on first-order shear deformation theory and subjected to lateral thermal shock loads. The beam is assumed to be graded across the thickness direction. The material properties across the thickness direction follow the volume fraction of the constitutive materials in power law form. The solution is obtained under the coupled thermoelastic assumption. The equation of motion and the conventional coupled energy equation are simultaneously solved to obtain the transverse deflection and temperature distribution in the beam. The governing partial differential equations are solved using the finite Fourier transformation method. Using the Laplace transform, the unknown variables are obtained in the Laplace domain. Applying the analytical Laplace inverse method, the solution in the time domain is derived. Results are presented for different power law indices and the coupling coefficients for a beam with simply supported boundary conditions. The results are validated with data reported in the literature.

1. Introduction

Recently developed functionally graded materials (FGM) show promise for their adaptability to high temperature environments, and have thus attracted international attention. Therefore, it is desirable to analyze FGM structures subjected to thermal loadings such as thermal shock, which have a wide range of applications in engineering and science. Very rapid thermal processes, under the action of a thermal shock are interesting from the standpoint of thermoelasticity. Under thermal shock, the characteristic times of structural and thermal disturbances are of comparable magnitudes, the equations of motion of a structure are coupled with the energy equation, and the solution of the coupled system of equations provides the stress and temperature fields.

The equations for a coupled thermoelastic beam, including the effects of the shear deformation and rotatory inertia, are derived in [Jones 1966]. McQuillen and Brull [1970] presented an analytical solution for the dynamic thermoelastic response of cylindrical shells using the variational theorem. The coupled thermally induced vibrations of the Euler–Bernoulli and Timoshenko beams with one-dimensional heat conduction are investigated in [Seibert and Rice 1973]. The coupled thermoelasticity of beams made of homogeneous and isotropic material is discussed in [Massalas and Kalpakidis 1983; 1984]. The analytical solution of the coupled thermoelasticity of beams with the Euler–Bernoulli assumption is given in the first of these papers, that with the Timoshenko assumption in the second. In the treatment of these problems, a linear approximation for temperature variation across the thickness direction of the beam is

Keywords: functionally graded material, thermal shock, first-order shear deformation theory, coupled thermoelasticity, finite Fourier transformation method.

considered. Eslami and Vahedi [1988] studied the one-dimensional coupled thermoelasticity problem of rods with the classical coupled thermoelastic assumption using the Galerkin finite element method.

A finite element coupled thermoelastic analysis of composite Timoshenko beams is given in [Maruthi Rao and Sinha 1997], where the temperature variation across the thickness direction is neglected. The coupled thermoelastic behavior of shells of revolution is analyzed in [Eslami et al. 1999]. Manoach and Ribeiro [2004] developed a numerical procedure to study the coupled large amplitude thermoelastic vibrations of the Timoshenko beams subjected to the thermal and mechanical loads using finite difference approximations and modal coordinate transformations. Sankar [2001; Sankar and Tzeng 2002] considered an FGM Euler beam and computed the thermal stresses based on the uncoupled thermoelastic assumption. The coupled thermoelasticity of functionally graded cylindrical shells is investigated in [Bahtui and Eslami 2007] using the Galerkin finite element method with two element types (C^0- and C^1-continuous) under impulsive thermal shock load. Babaei et al. [2008] present the behavior of an FGM Euler–Bernoulli beam under lateral thermal shock with the coupled thermoelastic assumption. The analysis is based on the Galerkin finite element method, using a C^1-continuous shape function, where the temperature change across the thickness direction is assumed to be linear and the axial inertia effect is neglected.

The aim of this paper is to present the analytical solution for the behavior of an FGM beam under lateral thermal shock with the coupled thermoelastic assumption. The analysis is based on first-order shear deformation theory. The mathematical functions of unknown variables such as lateral deflection and temperature are presented using the finite Fourier transformation and analytical Laplace inverse method. The time constants and frequencies of oscillations are presented for different power law indices. The novelty of the analytical solution presented in this work in comparison with prior researches is the absence of the unbalance of the members of matrices appearing in the numerical methods. Random dimensionless parameters are used to overcome this problem in previous studies about coupled thermoelasticity of FGM structures [Bahtui and Eslami 2007; Babaei et al. 2008]. Also, in analytical analysis, the coupled effect is stronger than perceived especially for long time periods, in comparison with the numerical methods.

2. Derivation of the governing equations

Consider a beam of rectangular cross section with length l, height h, and width b, as shown in Figure 1. Using first-order shear deformation theory, the displacement components are

$$u(x,z,t) = u_0 - z\psi_{,x}, \qquad w(x,z,t) = w(x,t), \tag{1}$$

where u is the axial displacement component, u_0 the displacement of a point on the reference plane, w is the lateral deflection, ψ is the rotation angle of the cross section with respect to the longitudinal axis,

Figure 1. The beam and coordinates.

t is the time variable, and z is measured across the thickness direction from the middle plane of the beam at $x = 0$. A comma in subscripts indicates partial differentiation.

The FGM profile across the thickness direction of the beam, made of ceramic and metal constituent materials, may be assumed to follow a power law form as

$$f(z) = f_m + f_{cm}\left(\frac{2z+h}{2h}\right)^n, \tag{2}$$

where f is any material property of the FGM, f_m is the metal property of FGM, $f_{cm} = f_c - f_m$, f_c being the ceramic property of FGM, and n is the power law index. The density, modulus of elasticity, coefficient of specific heat, coefficient of thermal expansion, and conduction coefficient may be assumed to follow the power law form, indicated by Equation (2).

Assuming that the beam material is linear elastic, the stress-strain relations for the FGM beam based on the assumed displacement components, including the shear deformation, are [Manoach and Ribeiro 2004]

$$\sigma_x = E(z)[\epsilon_x - \alpha(z)\theta], \qquad \sigma_{xz} = k_s G(z)\epsilon_{xz}, \tag{3}$$

where E is the modulus of elasticity, G is the shear modulus, k_s is the shear correction factor, α is the coefficient of thermal expansion, $\theta = T - T_0$ is the temperature change, and T_0 is the reference temperature.

The bending moment, the shear force, and the in-plane stress resultants are expressed by the stresses as follows:

$$M = \int_z \sigma_x z\, dz, \qquad Q = \int_z \sigma_{xz}\, dz, \qquad N = \int_z \sigma_x\, dz. \tag{4}$$

The temperature change across the thickness direction is assumed to be linear. This assumption is justified considering that the thickness of the beam is small with respect to its length [Massalas and Kalpakidis 1983; 1984] and thus

$$\theta(x, z, t) = \tfrac{1}{2}\big(\theta_1(x, t) + \theta_2(x, t)\big) + \frac{z}{h}\big(\theta_1(x, t) - \theta_2(x, t)\big) \tag{5}$$

where θ_1 and θ_2 are unknowns to be found across the beam's height and are coupled with the displacement components of the beam.

Equation of motion. The equations of motion of a beam based on first-order shear deformation theory are [Manoach and Ribeiro 2004]

$$N_{,x} = I_0 u_{0,tt} - I_1 \psi_{,tt}, \qquad M_{,x} - Q = I_1 u_{0,tt} - I_2 \psi_{,tt}, \qquad Q_{,x} = I_0 w_{,tt} - p(x, t), \tag{6}$$

where p is the applied surface lateral mechanical load, $I_i = \int_z \rho(z) z^i\, dz$ $(i = 0, 1, 2)$ is the mass moment of inertia, and ρ is the mass density of the beam.

Substituting (3), (4), (5) into (6), the equations of motion become

$$\begin{aligned} A_1 u_{0,xx} + A_2 \psi_{,xx} + A_3 \theta_{1,xx} + A_4 \theta_{2,xx} + A_5 u_{0,tt} + A_6 \psi_{,tt} &= 0, \\ B_1 u_{0,xx} + B_2 \psi_{,xx} + B_3 \psi + B_4 w_{,x} + B_5 \theta_{1,xx} + B_6 \theta_{2,xx} + B_7 u_{0,tt} + B_8 \psi_{,tt} &= 0, \\ C_1 \psi_{,x} + C_2 w_{,xx} + C_3 w_{,tt} &= 0, \end{aligned} \tag{7}$$

where the coefficients are given by

$$A_1=\int E(z)\,dz,\qquad A_3=\int\Big(-\frac{1}{2}-\frac{z}{h}\Big)E(z)\alpha(z)\,dz,\qquad A_5=-I_0,\qquad B_1=\int E(z)z\,dz,$$
$$A_2=\int -E(z)z\,dz,\qquad A_4=\int\Big(-\frac{1}{2}+\frac{z}{h}\Big)E(z)\alpha(z)\,dz,\qquad A_6=I_1,\qquad B_2=\int -E(z)z^2\,dz,$$
$$B_3=\int\frac{k_s}{2(1+\nu)}E(z)\,dz,\quad B_5=\int\Big(-\frac{z}{2}-\frac{z^2}{h}\Big)E(z)\alpha(z)\,dz,\quad B_7=-I_1,\quad C_1=B_3,\quad C_2=B_4,$$
$$B_4=\int\frac{k_s}{2(1+\nu)}E(z)\,dz,\quad B_6=\int\Big(-\frac{z}{2}+\frac{z^2}{h}\Big)E(z)\alpha(z)\,dz,\quad B_8=I_2,\quad C_3=-I_0.$$

Considering a beam with simply supported boundary conditions with initial zero deflection and zero velocity, the boundary and initial conditions may be assumed to be

$$\begin{aligned}
u_{0,x}(0,t)&=u_{0,x}(l,t)=0, && t>0,\\
\psi_{,x}(0,t)&=\psi_{,x}(l,t)=0, && t>0,\\
w(0,t)&=w(l,t)=0, && t>0,\\
u_0(x,0)&=\psi(x,0)=w(x,0)=0, && 0\le x\le l.
\end{aligned}\tag{8}$$

Energy equations. The first law of thermodynamics for heat conduction in the beam in coupled form is [Hetnarski and Eslami 2009]

$$(k\theta_{,i})_{,i}-\rho c_v\theta_{,t}-\alpha(3\lambda+2\mu)T_0(\epsilon_{ii})_{,t}=0,\quad i=1,2,3,\tag{9}$$

where k, c_v, α, and ϵ_{ii} are the thermal conductivity, specific heat, coefficient of linear thermal expansion, and normal strain tensor, respectively, and λ and μ are the Lamé constants. The energy equation for the beam based on first-order shear deformation theory is reduced to

$$\text{Res.}=k(z)\theta_{,xx}+(k(z)\theta_{,z})_{,z}-\rho(z)c_v(z)\theta_{,t}-\alpha(z)E(z)T_0[u_{0,xt}-z\psi_{,xt}]=0.\tag{10}$$

The thermal boundary conditions may be assumed in form of an applied heat flux q, convection h_c, or specified temperature shock on the upper or lower surfaces of the beam. The energy equation is obtained assuming that the upper surface of the beam is exposed to a known heat flux $q(x,t)$ and the lower surface is under convection to the ambient with coefficient h_c.

The beam is initially assumed to be at ambient temperature and the thermal boundary and initial conditions are assumed as

$$\theta(0,t)=\theta(l,t)=0,\quad t>0,\qquad \theta(x,0)=0,\quad 0\le x\le l.\tag{11}$$

Using (10), the residue, Res., of the energy equation may be made orthogonal with respect to dz and $z\,dz$ to provide two independent equations for two independent functions θ_1 and θ_2 as [McQuillen and Brull 1970]

$$\begin{aligned}
D_1\theta_{1,xx}+D_2\theta_{2,xx}+D_3\theta_{1,t}+D_4\theta_{2,t}+D_5u_{0,xt}+D_6\psi_{,xt}+D_7\theta_2+D_8q(x,t)&=0,\\
E_1\theta_{1,xx}+E_2\theta_{2,xx}+E_3\theta_1+E_4\theta_2+E_5\theta_{1,t}+E_6\theta_{2,t}+E_7u_{0,xt}+E_8\psi_{,xt}+E_9\theta_2+E_{10}q(x,t)&=0,
\end{aligned}\tag{12}$$

where the coefficients are given by

$$D_1 = \int\left(\frac{1}{2} + \frac{z}{h}\right)K(z)\,dz, \qquad D_3 = \int\left(-\frac{1}{2} - \frac{z}{h}\right)\rho(z)c_v(z)\,dz, \qquad D_5 = \int -E(z)\alpha(z)T_0\,dz,$$

$$D_2 = \int\left(\frac{1}{2} - \frac{z}{h}\right)K(z)\,dz, \qquad D_4 = \int\left(-\frac{1}{2} + \frac{z}{h}\right)\rho(z)c_v(z)\,dz, \qquad D_6 = \int E(z)\alpha(z)T_0 z\,dz,$$

$$E_1 = \int\left(\frac{z}{2} + \frac{z^2}{h}\right)K(z)dz, \qquad E_3 = \int -\frac{K(z)}{h}dz, \qquad D_7 = -h_c,$$

$$E_2 = \int\left(\frac{z}{2} - \frac{z^2}{h}\right)K(z)dz, \qquad E_4 = \int \frac{K(z)}{h}dz, \qquad D_8 = 1,$$

$$E_5 = \int\left(-\frac{z}{2} - \frac{z^2}{h}\right)\rho(z)c_v(z)dz, \qquad E_7 = \int -E(z)\alpha(z)zT_0dz, \qquad E_9 = -\frac{h}{2}h_c,$$

$$E_6 = \int\left(-\frac{z}{2} + \frac{z^2}{h}\right)\rho(z)c_v(z)dz, \qquad E_8 = \int E(z)\alpha(z)T_0z^2dz, \qquad E_{10} = \frac{h}{2}.$$

3. Solution procedure

To solve the simultaneous governing equations, dimensionless values are defined as

$$\bar{u}_0 = \frac{k_c}{q_{\text{avg}}\alpha_c l^2}u_0, \quad \bar{\psi} = \frac{k_c}{q_{\text{avg}}\alpha_c l}\psi, \quad \bar{w} = \frac{k_c}{q_{\text{avg}}\alpha_c l^2}w, \quad \bar{x} = \frac{x}{l}, \quad \bar{t} = \frac{\kappa_c}{h^2}t, \quad \bar{\theta} = \frac{k_c}{q_{\text{avg}}\alpha_c l T_0}\theta, \tag{13}$$

where q_{avg} and κ_c are, respectively, the average heat flux at the top of the beam and the thermal diffusivity. The bar indicates dimensionless parameters.

Using the dimensionless parameters, the five coupled governing equations are

$$\begin{aligned}
a_1\bar{u}_{0,\bar{x}\bar{x}} + a_2\bar{\psi}_{,\bar{x}\bar{x}} + a_3\bar{\theta}_{1,\bar{x}\bar{x}} + a_4\bar{\theta}_{2,\bar{x}\bar{x}} + a_5\bar{u}_{0,\bar{t}\bar{t}} + a_6\bar{\psi}_{,\bar{t}\bar{t}} &= 0,\\
b_1\bar{u}_{0,\bar{x}\bar{x}} + b_2\bar{\psi}_{,\bar{x}\bar{x}} + b_3\bar{\psi} + b_4\bar{w}_{,\bar{x}} + b_5\bar{\theta}_{1,\bar{x}\bar{x}} + b_6\bar{\theta}_{2,\bar{x}\bar{x}} + b_7\bar{u}_{0,\bar{t}\bar{t}} + b_8\bar{\psi}_{,\bar{t}\bar{t}} &= 0,\\
c_1\bar{\psi}_{,\bar{x}} + c_2\bar{w}_{,\bar{x}\bar{x}} + c_3\bar{w}_{,\bar{t}\bar{t}} &= 0,\\
d_1\bar{\theta}_{1,\bar{x}\bar{x}} + d_2\bar{\theta}_{2,\bar{x}\bar{x}} + d_3\bar{\theta}_{1,\bar{t}} + d_4\bar{\theta}_{2,\bar{t}} + d_5\bar{u}_{0,\bar{x}\bar{t}} + d_6\bar{\psi}_{,\bar{x}\bar{t}} + d_7\bar{\theta}_2 + d_8 q(\bar{x},\bar{t}) &= 0,\\
e_1\bar{\theta}_{1,\bar{x}\bar{x}} + e_2\bar{\theta}_{2,\bar{x}\bar{x}} + e_3\bar{\theta}_1 + e_4\bar{\theta}_2 + e_5\bar{\theta}_{1,\bar{t}} + e_6\bar{\theta}_{2,\bar{t}} + e_7\bar{u}_{0,\bar{x}\bar{t}} + e_8\bar{\psi}_{,\bar{x}\bar{t}} + e_9\bar{\theta}_2 + e_{10}q(\bar{x},\bar{t}) &= 0,
\end{aligned} \tag{14}$$

where the as, bs, cs, ds, and es are dimensionless constants of the coupled equations. Simultaneous solution of these equations provides the distribution of the displacement components of the beam and the temperature variables θ_1 and θ_2.

Regarding the boundary conditions given by (8) and (11), to solve (14), the finite Fourier transformation can be used to obtain

$$\bar{u}_{0m}(\bar{t}) = \int_0^1 \bar{u}_0(\bar{x},\bar{t})\cos(m\pi\bar{x})\,d\bar{x}, \quad \bar{\psi}_m(\bar{t}) = \int_0^1 \bar{\psi}(\bar{x},\bar{t})\cos(m\pi\bar{x})\,d\bar{x}, \quad \bar{w}_m(\bar{t}) = \int_0^1 \bar{w}(\bar{x},\bar{t})\sin(m\pi\bar{x})\,d\bar{x},$$

$$\bar{\theta}_{1m}(\bar{t}) = \int_0^1 \bar{\theta}_1(\bar{x},\bar{t})\sin(m\pi\bar{x})\,d\bar{x}, \quad \bar{\theta}_{2m}(\bar{t}) = \int_0^1 \bar{\theta}_2(\bar{x},\bar{t})\sin(m\pi\bar{x})\,d\bar{x}, \tag{15}$$

where $m = 1, 3, 5, \ldots$.

The solutions given by (15) automatically satisfy the boundary conditions, (8) and (11). Based on Fourier series theory, the inverse transformation can be expressed by

$$\bar{u}_0(\bar{x},\bar{t}) = 2\sum_m \bar{u}_{0m}(\bar{t})\cos(m\pi\bar{x}),\quad \bar{\psi}(\bar{x},\bar{t}) = 2\sum_m \bar{\psi}_m(\bar{t})\cos(m\pi\bar{x}),\quad \bar{\omega}(\bar{x},\bar{t}) = 2\sum_m \bar{\omega}_m(\bar{t})\sin(m\pi\bar{x}),$$
$$\bar{\theta}_1(\bar{x},\bar{t}) = 2\sum_m \bar{\theta}_{1m}(\bar{t})\sin(m\pi\bar{x}),\quad \bar{\theta}_2(\bar{x},\bar{t}) = 2\sum_m \bar{\theta}_{2m}(\bar{t})\sin(m\pi\bar{x}), \tag{16}$$

where the sum is all over m odd and positive. Applying a step function heat flux of intensity q to the upper beam surface, the Fourier transformation of (14), considering the initial conditions (8) and (11), yields

$$\begin{aligned}
-r^2a_1\bar{u}_{0m} - r^2a_2\bar{\psi}_m + ra_3\bar{\theta}_{1m} + ra_4\bar{\theta}_{2m} + a_5\bar{u}_{0m,\bar{t}\bar{t}} + a_6\bar{\psi}_{m,\bar{t}\bar{t}} &= 0,\\
-r^2b_1\bar{u}_{0m} - r^2b_2\bar{\psi}_m + +b_3\bar{\psi}_m + rb_4\bar{\omega}_m + rb_5\bar{\theta}_{1m} + rb_6\bar{\theta}_{2m} + b_7\bar{u}_{0m,\bar{t}\bar{t}} + b_8\bar{\psi}_{m,\bar{t}\bar{t}} &= 0,\\
-rc_1\bar{\psi}_m - r^2c_2\bar{\omega}_m + c_3\bar{\omega}_{m,\bar{t}\bar{t}} &= 0,\\
-r^2d_1\bar{\theta}_{1m} - r^2d_2\bar{\theta}_{2m} + d_3\bar{\theta}_{1m,\bar{t}} + d_4\bar{\theta}_{2m,\bar{t}} - rd_5\bar{u}_{0m,\bar{t}} - rd_6\bar{\psi}_{m,\bar{t}} + d_7\bar{\theta}_{2m} + \frac{2d_8}{r}q &= 0,\\
-r^2e_1\bar{\theta}_{1m} - r^2e_2\bar{\theta}_{2m} + e_3\bar{\theta}_{1m} + e_4\bar{\theta}_{2m} + e_5\bar{\theta}_{1m,\bar{t}} + e_6\bar{\theta}_{2m,\bar{t}} - re_7\bar{u}_{0m,\bar{t}} - re_8\bar{\psi}_{m,\bar{t}} + e_9\bar{\theta}_{2m} + \frac{2e_{10}}{r}q &= 0,
\end{aligned} \tag{17}$$

where $r = m\pi$.

Laplace transform. The system of coupled equations (17) are functions of the Fourier parameter m and time t. The solution presented in this paper is obtained by the finite Fourier transformation, where time is eliminated using the Laplace transform. Once the solution in the space domain is obtained, an analytical scheme is used for the inverse Laplace transformation to find the final solution in the real time domain. Applying the Laplace transform to (17) gives

$$\begin{aligned}
-r^2a_1\bar{U}_{0m} - r^2a_2\bar{\Psi}_m + ra_3\bar{\Theta}_{1m} + ra_4\bar{\Theta}_{2m} + a_5s^2\bar{U}_{0m} + a_6s^2\bar{\Psi}_m &= 0,\\
-r^2b_1\bar{U}_{0m} - r^2b_2\bar{\Psi}_m + +b_3\bar{\Psi}_m + rb_4\bar{W}_m + rb_5\bar{\Theta}_{1m} + rb_6\bar{\Theta}_{2m} + b_7s^2\bar{U}_{0m} + b_8s^2\bar{\Psi}_m &= 0,\\
-rc_1\bar{\Psi}_m - r^2c_2\bar{W}_m + c_3s^2\bar{W}_m &= 0,\\
-r^2d_1\bar{\Theta}_{1m} - r^2d_2\bar{\Theta}_{2m} + d_3s\bar{\Theta}_{1m} + d_4s\bar{\Theta}_{2m} - rd_5s\bar{U}_{0m} - rd_6s\bar{\Psi}_m + d_7\bar{\Theta}_{2m} + \frac{2d_8}{rs}q &= 0,\\
-r^2e_1\bar{\Theta}_{1m} - r^2e_2\bar{\Theta}_{2m} + e_3\bar{\Theta}_{1m} + e_4\bar{\Theta}_{2m} + e_5s\bar{\Theta}_{1m} + e_6s\bar{\Theta}_{2m}&\\
-re_7s\bar{U}_{0m} - re_8s\bar{\Psi}_m + e_9\bar{\Theta}_{2m} + \frac{2e_{10}}{rs}q &= 0,
\end{aligned} \tag{18}$$

where s is the Laplace transform parameter and $\bar{U}_{0m} = L[\bar{u}_{0m}]$, $\bar{\Psi}_m = L[\bar{\psi}_m]$, $\bar{W}_m = L[\bar{\omega}_m]$, and $\bar{\Theta}_{im} = L[\bar{\theta}_{im}]$ for $i = 1, 2$, where L stands for the Laplace operator. Denoting by

$$\langle F_{m_j}\rangle = \langle \bar{U}_{0m}\ \ \bar{\Psi}_m\ \ \bar{W}_m\ \ \bar{\Theta}_{1m}\ \ \bar{\Theta}_{2m}\rangle \tag{19}$$

the solution for the unknown variables in (18), in the Laplace transformation domain we obtain

$$F_{m_j}(s) = \frac{Q_{m_j}(s)}{P_{m_j}(s)}, \tag{20}$$

where $Q_{m_j}(s)$ and $P_{m_j}(s)$ are polynomial functions of s. As an example, the lateral deflection of the beam in the Laplace domain for the coupled assumption (d_5, d_6, e_7, $e_8 \neq 0$) can be given as

$$\bar{W}_m = \frac{q_0 + q_1 s + q_2 s^2 + q_3 s^3}{s(p_0 + p_1 s + p_2 s^2 + p_3 s^3 + p_4 s^4 + p_5 s^5 + p_6 s^6 + p_7 s^7 + p_8 s^8)}, \tag{21}$$

where the qs and ps are coefficients obtained by solving the system of (18).

Carrying out analytically the inverse Laplace transform of (20) [Massalas and Kalpakidis 1983; 1984], we obtain solutions for the unknown variables in the real physical time domain:

$$f_{m_j}(m, \bar{t}) = \sum_{\gamma=1}^{n_p} \frac{Q_{m_j}(s_{p_\gamma})}{P'_{m_j}(s_{p_\gamma})} e^{s_{p_\gamma}\bar{t}}, \tag{22}$$

where

$$\langle f_{m_j} \rangle = \langle u_{0m} \;\; \psi_m \;\; w_m \;\; \theta_{1m} \;\; \theta_{2m} \rangle,$$

the s_{p_γ} are the roots of $P_{m_j}(s)$, and n_p is the number of roots. A prime indicates a derivative with respect to s.

Using (16) and (22), the unknown variable functions are obtained in the space variable x and time t. As an example, the lateral deflection function is computed as

$$\begin{gathered}\bar{w}(\bar{x}, \bar{t}) = 2 \sum_{m=1,3,\ldots}^{\infty} \bar{w}_m(m, \bar{t}) \sin(m\pi\bar{x}) = 2 \sum_{m=1,3,\ldots}^{\infty} \sum_{\gamma=1}^{n_p} \frac{q_0 + q_1 s_{p_\gamma} + q_2 s_{p_\gamma}^2 + q_3 s_{p_\gamma}^3}{P_{\bar{w}}(s_{p_\gamma})} e^{s_{p_\gamma}\bar{t}} \sin(m\pi\bar{x}), \\ P_{\bar{w}} = p_0 + 2p_1 s_{p_\gamma} + 3p_2 s_{p_\gamma}^2 + 4p_3 s_{p_\gamma}^3 + 5p_4 s_{p_\gamma}^4 + 6p_5 s_{p_\gamma}^5 + 7p_6 s_{p_\gamma}^6 + 8p_7 s_{p_\gamma}^7 + 9p_8 s_{p_\gamma}^8.\end{gathered} \tag{23}$$

Using (16) and (22), and considering $m = 1$, the dimensionless functions for the midlength lateral deflection w, upper side temperature θ_1 at the midpoint of the beam, maximum u_0, and rotation angle ψ at $\bar{x} = 0$ are obtained for the coupled and uncoupled assumptions. For the uncoupled assumption, where d_5, d_6, e_7, $e_8 = 0$, we obtain

$$\begin{aligned}\bar{w}_{uc}(0.5, \bar{t}) &= \acute{A}_1 + \acute{A}_2 e^{\tau_{uc_1}\bar{t}} + \acute{A}_3 e^{\tau_{uc_2}\bar{t}} + \acute{A}_4 \cos(\omega_{uc_1}\bar{t}) + \acute{A}_5 \sin(\omega_{uc_1}\bar{t}) \\ &\quad + \acute{A}_6 \cos(\omega_{uc_2}\bar{t}) + \acute{A}_7 \sin(\omega_{uc_2}\bar{t}) + \acute{A}_8 \cos(\omega_{uc_3}\bar{t}) + \acute{A}_9 \sin(\omega_{uc_3}\bar{t}), \\ \bar{\theta}_{1uc}(0.5, \bar{t}) &= \acute{B}_1 + \acute{B}_2 e^{\tau_{uc_1}\bar{t}} + \acute{B} e^{\tau_{uc_2}\bar{t}}, \\ \bar{u}_{0uc}(0, \bar{t}) &= \acute{C}_1 + \acute{C}_2 e^{\tau_{uc_1}\bar{t}} + \acute{C}_3 e^{\tau_{uc_2}\bar{t}} + \acute{C}_4 \cos(\omega_{uc_1}\bar{t}) + \acute{C}_5 \sin(\omega_{uc_1}\bar{t}) + \acute{C}_6 \cos(\omega_{uc_2}\bar{t}) \\ &\quad + \acute{C}_7 \sin(\omega_{uc_2}\bar{t}) + \acute{C}_8 \cos(\omega_{uc_3}\bar{t}) + \acute{C}_9 \sin(\omega_{uc_3}\bar{t}), \\ \bar{\psi}_{uc}(0, \bar{t}) &= \acute{D}_1 + \acute{D}_2 e^{\tau_{uc_1}\bar{t}} + \acute{D}_3 e^{\tau_{uc_2}\bar{t}} + \acute{D}_4 \cos(\omega_{uc_1}\bar{t}) + \acute{D}_5 \sin(\omega_{uc_1}\bar{t}) + \acute{D}_6 \cos(\omega_{uc_2}\bar{t}) \\ &\quad + \acute{D}_7 \sin(\omega_{uc_2}\bar{t}) + \acute{D}_8 \cos(\omega_{uc_3}\bar{t}) + \acute{D}_9 \sin(\omega_{uc_3}\bar{t}),\end{aligned} \tag{24}$$

where the τ_{uc_i} are dimensionless time constants, the ω_{uc_i} are dimensionless oscillation frequencies, and the $\acute{A}$, $\acute{B}$, $\acute{C}$, $\acute{D}$ are dimensionless constants. Similarly, for the coupled assumption,

$$
\begin{aligned}
\bar{w}_c(0.5,\bar{t}) &= \tilde{A}_1 + \tilde{A}_2 e^{\tau_{c_1}\bar{t}} + \tilde{A}_3 e^{\tau_{c_2}\bar{t}} + e^{\tau_{c_3}\bar{t}}\big(\tilde{A}_4\cos(\omega_{c_1}\bar{t}) + \tilde{A}_5\sin(\omega_{c_1}\bar{t})\big)\\
&\quad + e^{\tau_{c_4}\bar{t}}\big(\tilde{A}_6\cos(\omega_{c_2}\bar{t}) + \tilde{A}_7\sin(\omega_{c_2}\bar{t})\big) + e^{\tau_{c_5}\bar{t}}\big(\tilde{A}_8\cos(\omega_{c_3}\bar{t}) + \tilde{A}_9\sin(\omega_{c_3}\bar{t})\big),\\
\bar{\theta}_{1c}(0.5,\bar{t}) &= \tilde{B}_1 + \tilde{B}_2 e^{\tau_{c_1}\bar{t}} + \tilde{B}_3 e^{\tau_{c_2}\bar{t}} + e^{\tau_{c_3}\bar{t}}\big(\tilde{B}_4\cos(\omega_{c_1}\bar{t}) + \tilde{B}_5\sin(\omega_{c_1}\bar{t})\big)\\
&\quad + e^{\tau_{c_4}\bar{t}}\big(\tilde{B}_6\cos(\omega_{c_2}\bar{t}) + \tilde{B}_7\sin(\omega_{c_2}\bar{t})\big) + e^{\tau_{c_5}\bar{t}}\big(\tilde{B}_8\cos(\omega_{c_3}\bar{t}) + \tilde{B}_9\sin(\omega_{c_3}\bar{t})\big),\\
\bar{u}_{0c}(0,\bar{t}) &= \tilde{C}_1 + \tilde{C}_2 e^{\tau_{c_1}\bar{t}} + \tilde{C}_3 e^{\tau_{c_2}\bar{t}} + e^{\tau_{c_3}\bar{t}}\big(\tilde{C}_4\cos(\omega_{c_1}\bar{t}) + \tilde{C}_5\sin(\omega_{c_1}\bar{t})\big)\\
&\quad + e^{\tau_{c_4}\bar{t}}\big(\tilde{C}_6\cos(\omega_{c_2}\bar{t}) + \tilde{C}_7\sin(\omega_{c_2}\bar{t})\big) + e^{\tau_{c_5}\bar{t}}\big(\tilde{C}_8\cos(\omega_{c_3}\bar{t}) + \tilde{C}_9\sin(\omega_{c_3}\bar{t})\big),\\
\bar{\psi}_c(0,\bar{t}) &= \tilde{D}_1 + \tilde{D}_2 e^{\tau_{c_1}\bar{t}} + \tilde{D}_3 e^{\tau_{c_2}\bar{t}} + e^{\tau_{c_3}\bar{t}}\big(\tilde{D}_4\cos(\omega_{c_1}\bar{t}) + \tilde{D}_5\sin(\omega_{c_1}\bar{t})\big)\\
&\quad + e^{\tau_{c_4}\bar{t}}\big(\tilde{D}_6\cos(\omega_{c_2}\bar{t}) + \tilde{D}_7\sin(\omega_{c_2}\bar{t})\big) + e^{\tau_{c_5}\bar{t}}\big(\tilde{D}_8\cos(\omega_{c_3}\bar{t}) + \tilde{D}_9\sin(\omega_{c_3}\bar{t})\big),
\end{aligned}
\tag{25}
$$

where the symbols have a similar meaning as in the uncoupled case. Therefore, it can be found from (24) and (25) that the coupling between the strain and temperature fields causes the damping effect on the dimensionless lateral deflection, w.

4. Results

To validate the formulations, the results of this paper are compared with the analytical solution of a homogeneous beam reported in [Massalas and Kalpakidis 1983]. An aluminum beam of length 0.25 m and height 0.0022 m with simply supported boundary conditions is assumed. The ends of the beam are assumed to be at ambient temperature $T_0 = 293$ K. The upper surface of the beam is exposed to a step function heat flux, while the lower surface is assumed to be thermally insulated. Figure 2 shows the midpoint lateral deflection history of the heated beam for the coupled thermoelasticity assumptions reported in [Massalas and Kalpakidis 1983] and the present study. Close agreements are observed between the two studies.

Consider an FGM beam with ceramic upper surface and metal lower surface. The material properties of metal and ceramic are given in Table 1. The mechanical boundary conditions at the ends of the beam are assumed to be simply supported. The thermal boundary conditions at the ends of the beam are assumed to be at ambient temperature at $T_0 = 293$ K. The upper side of the beam is subjected to a step function thermal shock while the lower side is subjected to convection to the surrounding ambient with coefficient $h_c = 10000\,\mathrm{W/m^2K}$.

Metal: Ti-6Al-4V	Ceramic: ZrO_2
$E_m = 66.2$ GPa	$E_c = 117.0$ GPa
$\nu = 0.322$	$\nu = 0.322$
$\alpha_m = 10.3 \times 10^{-6}$/K	$\alpha_c = 7.11 \times 10^{-6}$/K
$\rho_m = 4.41 \times 10^3$ kg/m^3	$\rho_c = 5.6 \times 10^3$ kg/m^3
$k_m = 18.1$ W/(m·K)	$k_c = 2.036$ W/(m·K)
$c_m = 808.3$ J/(kg·K)	$c_c = 615.6$ J/(kg·K)

Table 1. Material properties of metal and ceramic constituents.

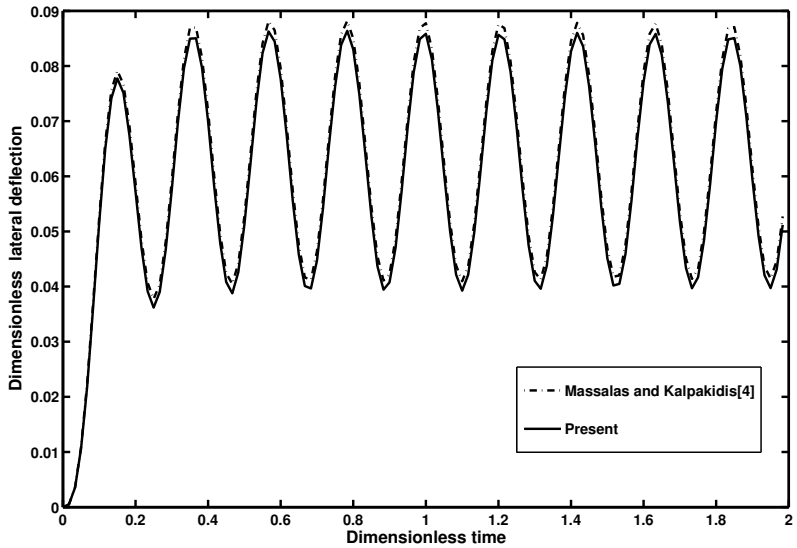

Figure 2. Lateral deflection history of an aluminum beam at midpoint with the coupled thermoelasticity assumption.

To compare the results with the numerical solutions presented by Babaei et al. [2008] for the FGM beam when $n = 0$, and $h/l = 0.001$, Figure 3 is plotted for the midpoint lateral deflection history for the uncoupled thermoelasticity case. It can be observed that the numerical solution had reasonable agreement with the present exact solution. The analytical solution presented in this work doesn't have the difficulties of numerical methods such as the unbalance of the members of matrices due to coupling between the strain and temperature fields and a time-consuming process.

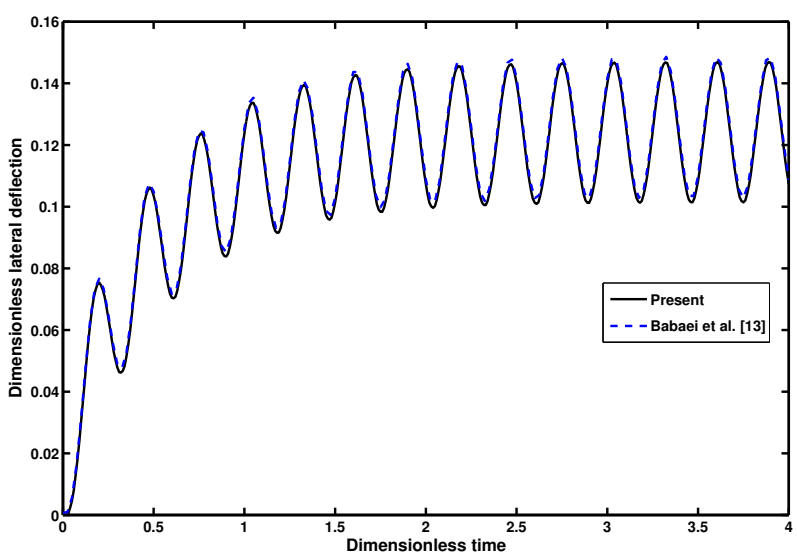

Figure 3. Comparison of the lateral deflection history at the midpoint of the FGM beam for $n = 0$ and $h/l = 0.001$.

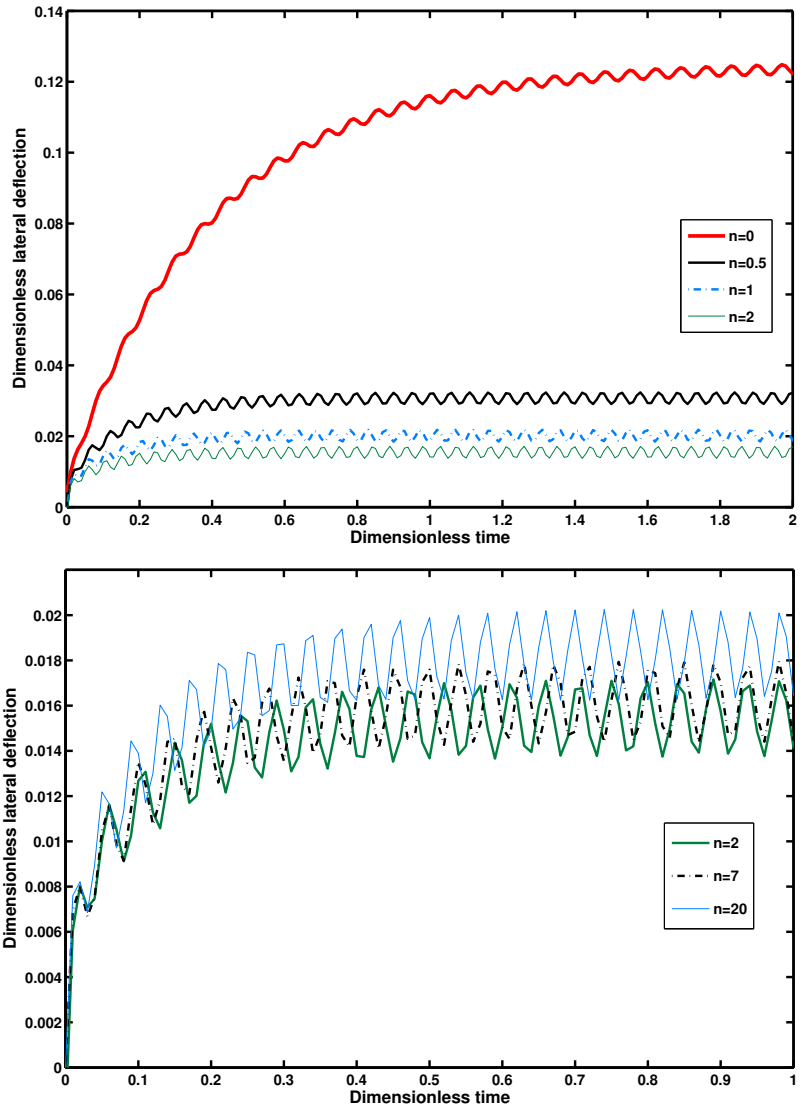

Figure 4. Lateral deflection history at the midpoint of the beam for different power law indices.

The next few figures show the effect of the power law index of the functionally graded beam in the uncoupled case. The maximum lateral deflection, frequency, and lateral amplitude of the FGM beam vibration due to the thermal shock depend on the mechanical and thermal properties of the beam. Thus, when n changes, the FGM beam shows different behaviors. Figure 4 plots the lateral deflection at midlength versus time for different values of the power law index n. The value $n = 0$ corresponds to a pure ceramic beam. We see in Figure 4, top, that as n increases, the midpoint lateral deflection of the FGM beam decreases due to the decline of the temperature gradient in the beam. However, this condition does not always continue. As shown in Figure 4, bottom, when $n > 1$, the difference in lateral deflection for different values of n becomes smaller with smaller amplitudes. Ceramic has a larger modulus of

n	τ_{uc_1}	τ_{uc_2}	ω_{uc_1}	ω_{uc_2}	ω_{uc_3}
0	−58.6014	−2.5144	538.2486		3.6757×10^7
0.5	−84.3941	−6.0998	507.8697	1.8224×10^5	3.5470×10^7
1	−98.4801	−7.0313	497.3527	1.7778×10^5	3.4484×10^7
2	−113.3725	−7.7118	492.1442	1.7282×10^5	3.3254×10^7
7	−131.8458	−8.3314	485.4957	1.6578×10^5	3.1632×10^7
20	−138.3074	−8.5187	472.9925	1.6288×10^5	3.1229×10^7

Table 2. Values of the dimensionless time constants and the dimensionless frequencies of oscillations for different power law indices in the uncoupled solution.

elasticity than metal, but a smaller coefficient of thermal expansion. This causes noncontinuous behavior in the maximum lateral deflection for FGM beams subjected to thermal shock. Furthermore, for larger power law indices which provide most metal rich FGM, the lateral deflection and oscillation frequency begin to slightly increase. In general, the lateral amplitude of vibration of the FGM beam due to the applied thermal shock is increased when the beam constituent materials change from the ceramic-rich to the metal-rich condition. Using (24), the dimensionless time constants and the dimensionless frequencies of oscillations are presented for different power law indices in Table 2.

From Table 2 we see that the frequency of the FGM beam vibration drops when the power law index n increases. Also, the diffusivity effect of the FGM beam is increased when the beam constituent materials change from the ceramic-rich to the metal-rich condition, that is when n is increased.

Figure 5 shows the temperature history at the upper side and the midlength of the beam. Due to the applied step function thermal shock, the beam temperature peaks to a maximum value, and then diffuses during the time. The figure shows that for the most metal rich FGM beams (higher values of n), the

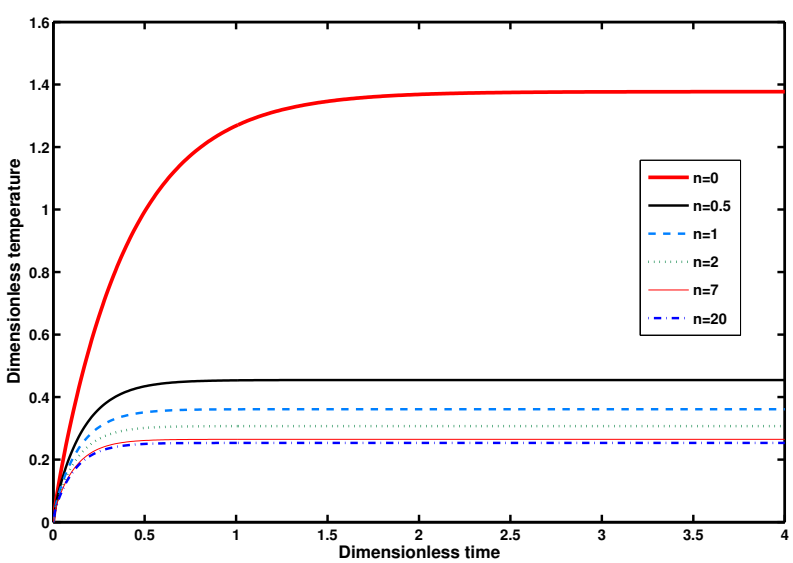

Figure 5. Temperature change history at the midpoint of the beam at the upper side for different power law indices.

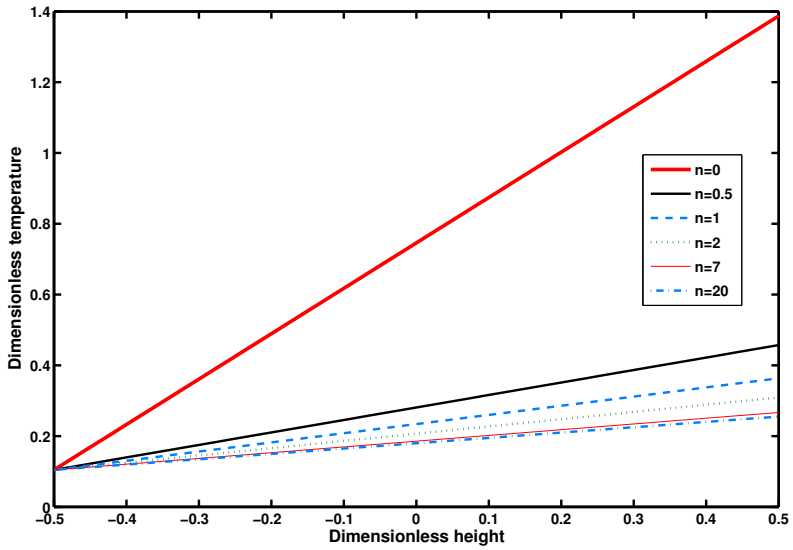

Figure 6. Temperature change distribution at the midpoint of the beam across the thickness direction at $\bar{t} = 3$ for different power law indices.

temperature distribution decreases in value due to the higher thermal conductivity of metal. Figure 6 shows the distribution of the temperature changes across the thickness direction at the midpoint of the beam at $\bar{t} = 3$. It is concluded that for higher values of n, the temperature distribution is changed slightly across the thickness of the FGM beam. By increasing the ceramic share of the beam, the gradient of temperature increases in value due to the lower thermal conductivity of ceramic.

Using (16) and (22), the expressions for the lateral deflection w and the upper surface temperature θ_1 at the midpoint of the beam can be obtained. In terms of the dimensionless quantities, and when $m = 1$, $n = 0$, and $h/l = 0.001$, the lateral deflection and the upper surface temperature at the midpoint of the beam for the coupled and coupled assumptions are

$$\begin{aligned}
\bar{w}_{uc}(0.5,\bar{t}) &= 0.1290 - 6.6592\cdot 10^{-3} e^{-29.6594\bar{t}} - 0.1094 e^{-1.9872\bar{t}} \\
&\quad -1.2936\cdot 10^{-2}\cos(22.0503\bar{t}) - 1.8817\cdot 10^{-2}\sin(22.0503\bar{t}) \\
&\quad +1.7574\cdot 10^{-24}\cos(1.4703\cdot 10^{7}\bar{t}) + 1.1840\cdot 10^{-19}\sin(1.4703\cdot 10^{7}\bar{t}), \\
\bar{w}_{c}(0.5,\bar{t}) &= 0.1290 - 6.6635\cdot 10^{-3} e^{-29.6531\bar{t}} - 0.1094 e^{-1.9862\bar{t}} \\
&\quad + e^{-2.4257\cdot 10^{-3}\bar{t}}\left(-1.2931\cdot 10^{-2}\cos(22.0526\bar{t}) - 1.8816\cdot 10^{-2}\sin(22.0526\bar{t})\right) \\
&\quad + e^{-1.2339\cdot 10^{-3}\bar{t}}\left(2.6551\cdot 10^{-18}\cos(2.432\cdot 10^{4}\bar{t}) + 1.1878\cdot 10^{-20}\sin(2.432\cdot 10^{4}\bar{t})\right) \\
&\quad + e^{-2.0487\cdot 10^{-8}\bar{t}}\left(1.7574\cdot 10^{-25}\cos(1.4703\cdot 10^{7}\bar{t}) + 1.1840\cdot 10^{-19}\sin(1.4703\cdot 10^{7}\bar{t})\right), \\
\bar{\theta}_{1uc}(0.5,\bar{t}) &= 0.7356 - 0.0355 e^{-29.6594\bar{t}} - 0.7001 e^{-1.9872\bar{t}}, \\
\bar{\theta}_{1c}(0.5,\bar{t}) &= 0.7356 - 0.0355^{-29.6531\bar{t}} - 0.7001 e^{-1.9862\bar{t}} \\
&\quad + e^{-2.4257\cdot 10^{-3}\bar{t}}\left(1.6513\cdot 10^{-5}\cos(22.0526\bar{t}) + 6.3336\cdot 10^{-6}\sin(22.0526\bar{t})\right) \\
&\quad + e^{-1.2339\cdot 10^{-3}\bar{t}}\left(-1.0203\cdot 10^{-11}\cos(2.432\cdot 10^{4}\bar{t}) + 1.2627\cdot 10^{-8}\sin(2.432\cdot 10^{4}\bar{t})\right) \\
&\quad + e^{-2.0487\cdot 10^{-8}\bar{t}}\left(3.7231\cdot 10^{-22}\cos(1.4703\cdot 10^{7}\bar{t}) + 1.7298\cdot 10^{-16}\sin(1.4703\cdot 10^{7}\bar{t})\right).
\end{aligned} \tag{26}$$

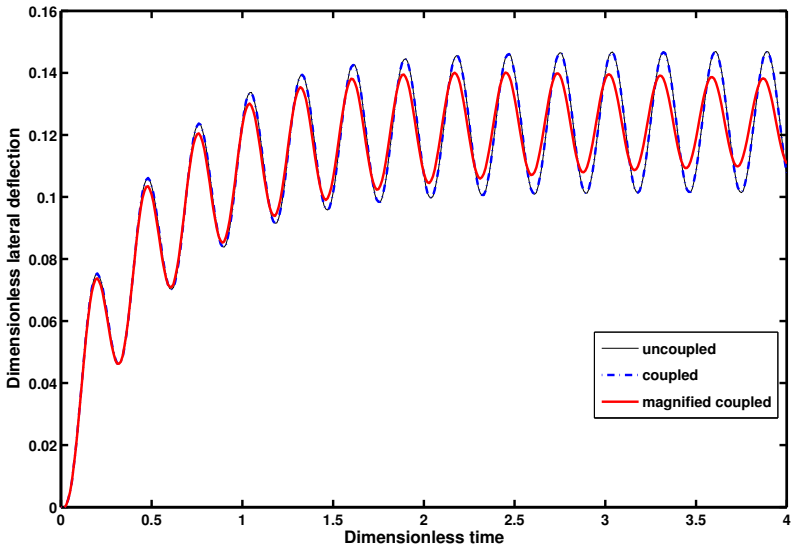

Figure 7. Lateral deflection history at the midpoint of the FGM beam for $n = 0$ and $h/l = 0.001$, showing the effects of coupling.

Investigating (26), one sees that the coupling between the strain and temperature fields has a damping effect on the dimensionless lateral deflection w. The plot of (26) for the lateral deflection history at the midpoint of a beam when $n = 0$, $h/l = 0.001$, and the coupling factors are $d_5 = -0.5027$, $d_6 = 0$, $e_7 = 0$, and $e_8 = 4.1891 \times 10^{-5}$, is shown in Figure 7. As shown in this figure the difference between the coupled and uncoupled solutions for the lateral deflection is negligible. For the magnified coupled solution, where the coupling coefficient is made 50 times larger, the amplitude of vibration increases and the frequency of vibration decreases, compared to the uncoupled solution, as time advances.

Figure 8 shows the lateral deflection history at the midpoint of an FGM beam ($n = 20$) with $h/l = 0.003125$, where the coupling factors are $d_5 = -0.1339$, $d_6 = 2.9444 \times 10^{-6}$, $e_7 = 9.4221 \times 10^{-4}$, and $e_8 = 3.5667 \times 10^{-5}$. Figure 9 shows the temperature history on the upper side of the FGM beam ($n = 20$) with $h/l = 0.003125$ for the coupled and uncoupled solutions, where no distinguishable difference is observed.

In general, the coupled and uncoupled thermoelasticity solutions of the structural problems do not have significant differences in the distribution of displacement and stress, except that for the coupled problems local stress and temperature wave fronts appear, which may cause structural damage. In addition, the coupled solution for the major part of the stress distribution (except around the wave front) is lower than that of the uncoupled solution. Now, the magnitudes of the stress and temperature wave fronts depend upon how short a time the thermal shock is applied. The shorter duration of the applied thermal shock, the higher the magnitude of the stress wave front becomes.

In Figures 7–9, however, wave fronts for the displacement and temperature do not appear. The reason is that the stress and temperature wave fronts appear in any structure under thermal shock. But, they are only detected when the solution is based on the generalized thermoelasticity equations. That is, when the flexural model is used, such as the beams, plates, and shells, the wave fronts do not appear in the

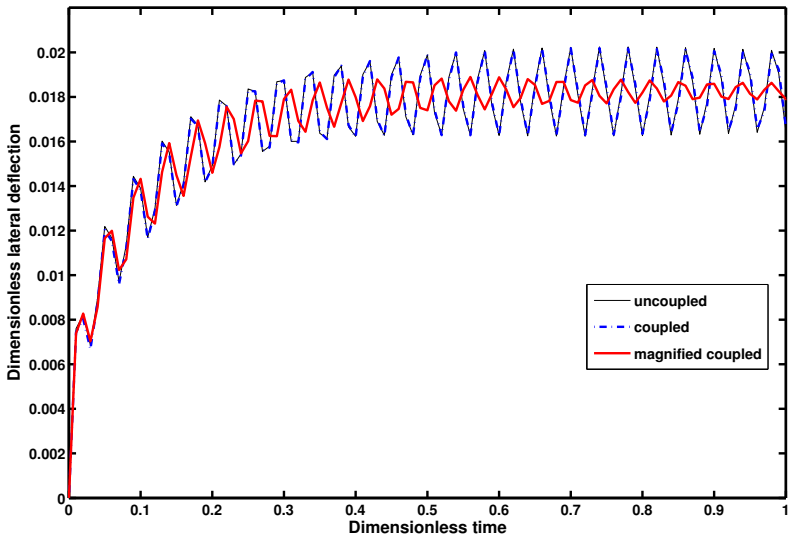

Figure 8. Lateral deflection history at the midpoint of the FGM beam for $n = 20$ and $h/l = 0.003125$, showing the effects of coupling.

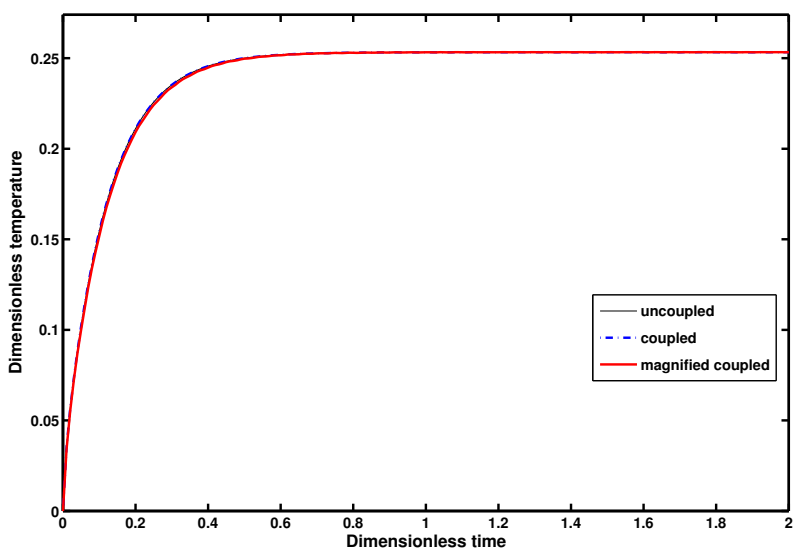

Figure 9. Temperature change history at the midpoint of the FGM beam at the upper side for $n = 20$ and $h/l = 0.003125$, showing the effects of coupling.

solution. The reason is simple, as we have lumped the stress through the thickness. Figure 9 for the temperature distribution does not show a wave front, as the classical coupled thermoelasticity theory is used in this paper, where the temperature equation is of parabolic type and the speed of propagation of the temperature

5. Conclusions

In the present paper, the coupled thermoelasticity of a beam based on first-order shear deformation theory with functionally graded material is investigated. The beam is subjected to a thermal shock of step function type on the upper side. The lower side of the beam is assumed to have convection to the surrounding ambient. Boundary conditions of the beam are taken to be simply supported, with ambient temperature at the ends of the beam. To solve the problem, the finite Fourier transformation is used. Moreover, to treat the time dependency, the Laplace transform technique is applied. The inverse Laplace transform is carried out analytically.

Results show that for larger values of power law indices, which provide the most metal rich FGM, the lateral deflection of an FGM beam due to a applied thermal shock does not decrease proportionally. There is an optimum value for the FGM parameter at which the beam's lateral deflection is minimum. By increasing the metal share of the FGM beam, the distribution of temperature changes slightly across the thickness of the beam. The amplitude of lateral vibration considerably increases as the aspect ratios of the beam decrease. Moreover, generally it can be said that there is no significant difference between the coupled and uncoupled solutions. However, the effect of coupling is in the form of damping. It decreases the amplitude of vibration and increase the frequency of the vibrations with the increase of time.

Acknowledgement

The authors thank the National Elite Foundation for the grant that was provided to support this research project.

References

[Babaei et al. 2008] M. H. Babaei, M. Abbasi, and M. R. Eslami, "Coupled thermoelasticity of functionally graded beams", *J. Therm. Stresses* **31**:8 (2008), 680–697.

[Bahtui and Eslami 2007] A. Bahtui and M. R. Eslami, "Coupled thermoelasticity of functionally graded cylindrical shells", *Mech. Res. Commun.* **34**:1 (2007), 1–18.

[Eslami and Vahedi 1988] M. R. Eslami and H. Vahedi, "Coupled thermoelasticity beam problems", *AIAA J.* **27**:5 (1988), 662–665.

[Eslami et al. 1999] M. R. Eslami, M. Shakeri, A. R. Ohadi, and B. Shiari, "Coupled thermoelasticity of shells of revolution: effect of normal stress and coupling", *AIAA J.* **37**:4 (1999), 496–504.

[Hetnarski and Eslami 2009] R. B. Hetnarski and M. R. Eslami, *Thermal stresses: advanced theory and applications*, Solid Mechanics and its Applications **158**, Springer, Dordrecht, 2009.

[Jones 1966] P. J. Jones, "Thermoelastic vibrations of a beam", *J. Acoust. Soc. Am.* **39**:3 (1966), 542–548.

[Manoach and Ribeiro 2004] E. Manoach and P. Ribeiro, "Coupled, thermoelastic, large amplitude vibrations of Timoshenko beams", *Int. J. Mech. Sci.* **46**:11 (2004), 1589–1606.

[Maruthi Rao and Sinha 1997] D. Maruthi Rao and P. K. Sinha, "Finite element coupled thermostructural analysis of composite beams", *Comput. Struct.* **63**:3 (1997), 539–549.

[Massalas and Kalpakidis 1983] C. V. Massalas and V. K. Kalpakidis, "Coupled thermoelastic vibrations of a simply supported beam", *J. Sound Vib.* **88**:3 (1983), 425–429.

[Massalas and Kalpakidis 1984] C. V. Massalas and V. K. Kalpakidis, "Coupled thermoelastic vibrations of a Timoshenko beam", *Int. J. Eng. Sci.* **22**:4 (1984), 459–465.

[McQuillen and Brull 1970] E. J. McQuillen and M. A. Brull, "Dynamic thermoelastic response of cylindrical shell", *J. Appl. Mech.* (*ASME*) **37**:3 (1970), 661–670.

[Sankar 2001] B. V. Sankar, "An elasticity solution for functionally graded beams", *Compos. Sci. Technol.* **61**:5 (2001), 689–696.

[Sankar and Tzeng 2002] B. V. Sankar and J. T. Tzeng, "Thermal stresses in functionally graded beams", *AIAA J.* **40**:6 (2002), 1228–1232.

[Seibert and Rice 1973] A. G. Seibert and J. S. Rice, "Coupled thermally induced vibrations of beams", *AIAA J.* **11**:7 (1973), 1033–1035.

Received 12 Mar 2009. Revised 19 Sep 2009. Accepted 21 Sep 2009.

MOSTAFA ABBASI: musan.abbasi@gmail.com
Mechanical Engineering Department, Amirkabir University of Technology, 424 Hafez Avenue, Tehran 15914, Iran
http://www.mostafabbasi.ir

MEHDY SABBAGHIAN: mehdys@bellsouth.net
Mechanical Engineering Department, Louisiana State University, Baton Rouge, LA 70803, United States

M. REZA ESLAMI: eslami@aut.ac.ir
Mechanical Engineering Department, Amirkabir University of Technology, 424 Hafez Avenue, Tehran 15914, Iran
http://me.aut.ac.ir/M.Eslami.htm